GSA Data Repository 2019006

Supplementary material

Fe-rich ferropericlase and magnesiowüstite inclusions reflecting diamond formation rather than ambient mantle

Paolo Nimis, Fabrizio Nestola, Mariangela Schiazza, Riccardo Reali, Giovanna Agrosì, Daniela Mele, Gioacchino Tempesta, Daniel Howell, Mark T. Hutchison, Richard Spiess

SAMPLE LOCATION

Diamond BZ270 derives from within a 30 km radius of the small Rio São Luiz, near the town of Juina. The sampling site for diamond JUc4 can be more precisely constrained to 261000 m E and 8708000 m N in WGS84 UTM-projected Zone 21S (Agrosi et al. 2017; Figure DR1).

METHODS

Micro-Computed X-ray Tomography

Micro-Computed X-ray Tomography (Cnudde and Boone, 2013) was carried out using a Scyscan 1172 microtomograph, located at the University of Bari (Italy). A 45-kV X-ray source was used with a current of 218 μA. A total of 1200 absorption radiographs were acquired over a 360 ° rotation with an angular step of 0.3 °. Random movement of the vertical axis and multiple-frame averaging were used to minimize the Poisson noise in the projection images. Beam hardening was reduced by the presence of a 0.5 mm Al-filter between the source and the detector. The nominal spatial resolution for the resulting model was 4.75 μm. The raw data were reconstructed into two-dimensional slice images using the software "NRecon, Skyscan, Belgium". Corrections for the beam-hardening effect and ring artifacts were also applied during the reconstruction process. Micro-CT data were analyzed using the software "CT-analyser, Skyscan, Belgium".

Cathodoluminescence

Cathodoluminescence images were collected on a Centaurus detector attached to a Hitachi S-3500N scanning electron microscope (SEM; School of Earth Sciences, University of Bristol). Samples were carbon coated prior to imaging. Accelerating voltages were varied between 10 and 20 kV to obtain the best quality images.

Electron microprobe analyses

Chemical analyses were carried out with a CAMECA SX-50 electron microprobe (IGG–CNR, Padua, Italy), equipped with four wavelength-dispersive spectrometers using one LIF, one PET, and two TAP

crystals. The following natural and synthetic materials were used as standards: for FM, diopside (for Ca and Si), albite (for Na), orthoclase (for K), and pure Al_2O_3, MgO, Cr_2O_3, Fe_2O_3, NiO, and $MnTiO_3$; for sulfides, pyrite (for S and Fe), pure metals (for Co, Ni, and Cr) and $MnTiO_3$ (for Mn). X-ray counts were converted into weight percent oxides or elements by using the CAMECA-PAP program. Analytical condition were a 1-μm electron beam, 20 kV accelerating voltage, 20 nA beam current, and a counting time of 10 s for peak and 10 s for background (i.e., 5 s on each side of the peak). Typical analytical uncertainties were better than ±1–2 relative % for major elements/oxides, better than ±10 relative % for minor elements/oxides with concentrations >0.2 wt%, and up to ±20 relative % for elements/oxides with lower concentrations. The analysis of the sulfide inclusions was hampered by their very small size and yielded low analytical totals (93.1–93.6 wt. %).

Single crystal X-ray diffractometry

The crystallographic orientation matrices of the FM inclusions and of their diamond hosts were determined using a prototype Supernova (Rigaku-Oxford Diffraction) X-ray single-crystal diffractometer equipped with an extremely brilliant micro-X-ray source focused to 0.12 mm (Mo Kα) and an extremely sensitive and no-noise 200 K Pilatus detector (Dectris). Due to the small unit cells of FM and diamond, there is nearly complete overlap in *d*-spacings between the most intense reflections 200 of FM and 111 of diamond, as well as further reflection overlaps. The best approach to distinguish FM from diamond in diffraction images is to consider the 220 and 111 reflections of the oxide (with *d*-spacing being about 2.4 and 1.5 Å), which do not overlap with any reflections of the diamond. Our XRD data also showed the presence of additional reflections, unrelated to either FM or diamond, which can be ascribed to the presence of magnesioferrite or magnetite exsolutions (Fig. DR2), an apparently common feature in FM inclusions in diamond (see Palot et al., 2016).

The orientations of the ferropericlase inclusions relative to their diamond hosts were calculated from the XRD orientation matrices with the OrientXplot software (Angel et al., 2015). High-quality unit-cell parameters were determined for four of the inclusions in diamond BZ270 by using a STOE STADI IV four-circle diffractometer (installed at the Department of Geosciences, University of Padua) operating at 50 kV and 40 mA, equipped with a point detector and controlled by the software SINGLE (Angel and Finger 2011), following the same approach used in Nestola et al. (2011). Accurate centering of the crystal under the X-ray beam was achieved by iterative adjustment of the crystal offset calculated by the software SINGLE. This procedure could not be applied to all inclusions, owing to an insufficient number of observed reflections. In such cases, lower-quality unit-cell parameters were obtained directly from the previously determined orientation matrices using the OrientXplot software (Angel et al., 2015). No reliable data could be obtained from the small inclusion n. 1 in diamond JUc4.

Complete diffraction intensity data were collected on the inclusions in diamond BZ270 with the Supernova diffractometer, by using a similar approach as used in Nestola et al. (2011). Data for three of the inclusions (n. 1, 2 and 3) were collected in situ when the inclusions were still completely enclosed in the diamond. Data for inclusions 4 and 5 were collected after further polishing, when the inclusions were exposed on surface. Data were collected up to $2\theta_{max} = 80°$ (working conditions 50 kV and 0.8 mA, exposure time 5 s for inclusions n. 1 and 2 and 15 s for inclusion n. 3). We were able to collect 25 unique reflections for inclusions n. 1, 2, 4 and 5, but only 12 for the smaller inclusion n. 3. Crystal structure refinements were performed using the software SHELXL (Sheldrick, 2008), using neutral atomic scattering factors for Mg and O and anisotropic thermal parameters; no contribution from other elements was considered, as EMPA of a

large number of FM inclusions extracted from Juina diamonds indicated that Fe and Mg typically represent more than 99% of the cations (Hutchison, 1997). The refinements for two of the inclusions were hampered by the small number of observed reflections (inclusion n. 3) and by the bad reflection profiles (inclusion n. 4), and were considered to be of unsatisfactory quality (e.g., thermal parameters, strongly correlated with the site occupancies, were lower than their uncertainties). The refinements for inclusions n. 1, 2 and 5 allowed us to calculate the site occupancy, from which the X_{Fe} values shown in Table 1 were calculated. Crystal structure refinements could not be performed on inclusions in diamond JUc4, because of low diffraction intensities (inclusion n. 1) or overlapping of diffraction reflections related to nearby inclusions (inclusions n. 2, 3 and 4). The latter issue was particularly critical owing to the similar crystallographic orientation among the inclusions.

EBSD Analysis

EBSD mapping was conducted at the Department of Geosciences, Padua using a NordlysNano EBSD camera (Oxford Instruments) mounted on a CamScan 2500 SEM equipped with an LaB6 source. Mapping was conducted at a 3-μm step size over a grid of 1005 x 698 points. Indexing of the EBSD patterns was accepted when at least eight Kikuchi bands were detected by the HKL Channel 5 software. The hit-rate was better than 90%. Noise correction of the EBSD-map was done using the standard Channel 5 software. After elimination of wild spikes, zero solutions were substituted with the orientation of neighboring grains according to an iterative process, which implied first substituting of zero solutions with the orientation of eight indexed neighboring grains, then with six and finally with four. Inverse Pole Figure (IPF) color coding was used to reveal mis-orientations within the EBSD map. The crystallographic orientation of the single EBSD data was plotted in lower hemisphere pole figures, using equal-area projections for the different crystallographic planes and directions (Fig. DR3).

EVALUATION OF FM CHEMICAL COMPOSITION

The chemical compositions of the studied inclusions were estimated on the basis of XRD data and, for inclusions exposed by polishing, determined by EMPA. The use of XRD data for this purpose is warranted by the fact that in FM inclusions extracted from Juina diamonds Fe and Mg typically represent more than 99% of the cations (Hutchison, 1997), which reduces the effective number of compositional variables to one (i.e., X_{Fe}). Two independent methods were used. One was based on a linear regression of compositional and unit-cell edge data at room conditions for stoichiometric synthetic FM (Fig. DR4), which yielded the equation $X_{Fe} = 8.441 \cdot a$ (Å) – 35.553. This equation reproduces the experimental X_{Fe} data with a maximum error of 0.02. For inclusions under residual pressure, a condition that occurs for several inclusions analyzed in situ within Juina diamonds (Hutchison, 1997), and for non-stoichiometric compositions, this method only provides minimum estimates of X_{Fe}. The second method is based on the structural refinement and evaluation of electron densities on the crystallographic sites (see above). This method is independent of residual pressure, but could only be applied to inclusions for which the highest-quality XRD could be obtained.

Inclusions in diamond BZ270 have unit-cell edges that are identical within error (Table DR2). Crystallographic site occupancies for inclusions n. 1 and 2, which were measured in situ, and n. 5, which was measured after exposing it by polishing, indicate X_{Fe} values of 0.31 to 0.36. These values are within error of those derived from equation $X_{Fe} = 8.441 \cdot a$ (Å) – 35.553 (Fig. DR2, Table 1). EMPA data for inclusions n. 4 and 5 (Table DR1) indicate a $(Mg_{0.65–0.66}Fe_{0.35–0.34})O$ composition, which is again within error of that

determined for inclusion n. 5 from XRD data (Fig. DR2, Table 1). The good agreement between chemical compositions estimated from independent XRD data and between those obtained from XRD and EMPA data indicates that the FM inclusions are nearly stoichiometric. It also indicates that the three inclusions are at virtually null pressure, probably due to stress release by cracking around the inclusions, plastic deformation or elastic relaxation during polishing.

The four studied FM inclusions in diamond JUc4 show larger and more variable unit-cell edges (Table DR2). Assuming no residual pressure also in this case, using the same X_{Fe} vs. a equation we calculate an X_{Fe} range of 0.43–0.64 (Table 1). In case of non-null residual pressure, these calculated X_{Fe} values would provide minimum estimates of the true X_{Fe} values.

TABLE DR1. ELECTRON MICROPROBE ANALYSES (WT. %) OF INCLUSIONS IN DIAMOND BZ270

Inclusion	n. of analyses	SiO_2	TiO_2	Al_2O_3	Cr_2O_3	FeO	MnO	NiO	MgO	CaO	Na_2O	K_2O	Total
FM n. 4	5	0.13(2)	<0.05	<0.05	0.35(4)	48.1(4)	0.16(1)	0.39(1)	51.0(4)	<0.03	<0.06	<0.03	100.1
FM n. 5	3	0.13(3)	<0.05	0.11(3)	0.37(1)	47.5(2)	0.14(1)	0.38(2)	52.2(2)	<0.03	<0.06	n.a.	100.8
		S	Fe	Mn	Co	Ni	Cr						
Sulfide	2	35.8(4)	56.5(2)	<0.05	0.13(2)	0.94(5)	<0.04						93.3*

Note: Numbers in parentheses indicate 1·σ uncertainties on the last digit.
*: low total due to small crystal size; n.a.: not analyzed.

TABLE DR2. SUMMARY OF CRYSTALLOGRAPHIC DATA FOR THE STUDIED FM INCLUSIONS.

Diamond	Inclusion	a (Å)	Angle between $(112)_{FM}$ and $(112)_{diam}$	Angle between $a_{i,FM}$ and $a_{i,diam}$
BZ270	1	4.2526(4)	1.3	5.1–7.3
	2	4.2531(3)	1.2	5.0–6.6
	3	4.253(5)	1.8	5.8–6.4
	4	4.2524(7)	1.0	5.7–7.7
	5	4.2534(2)	1.4	5.0–7.7
JUc4	2	4.280(5)	0.8	2.6–5.1
	3	4.264(5)	0.4	3.6–4.3
	4	4.263(7)	0.5	3.8–5.4
	5	4.288(3)	0.7	2.6–4.5

Note: Numbers in parentheses indicate 1·σ uncertainties on the last digit.

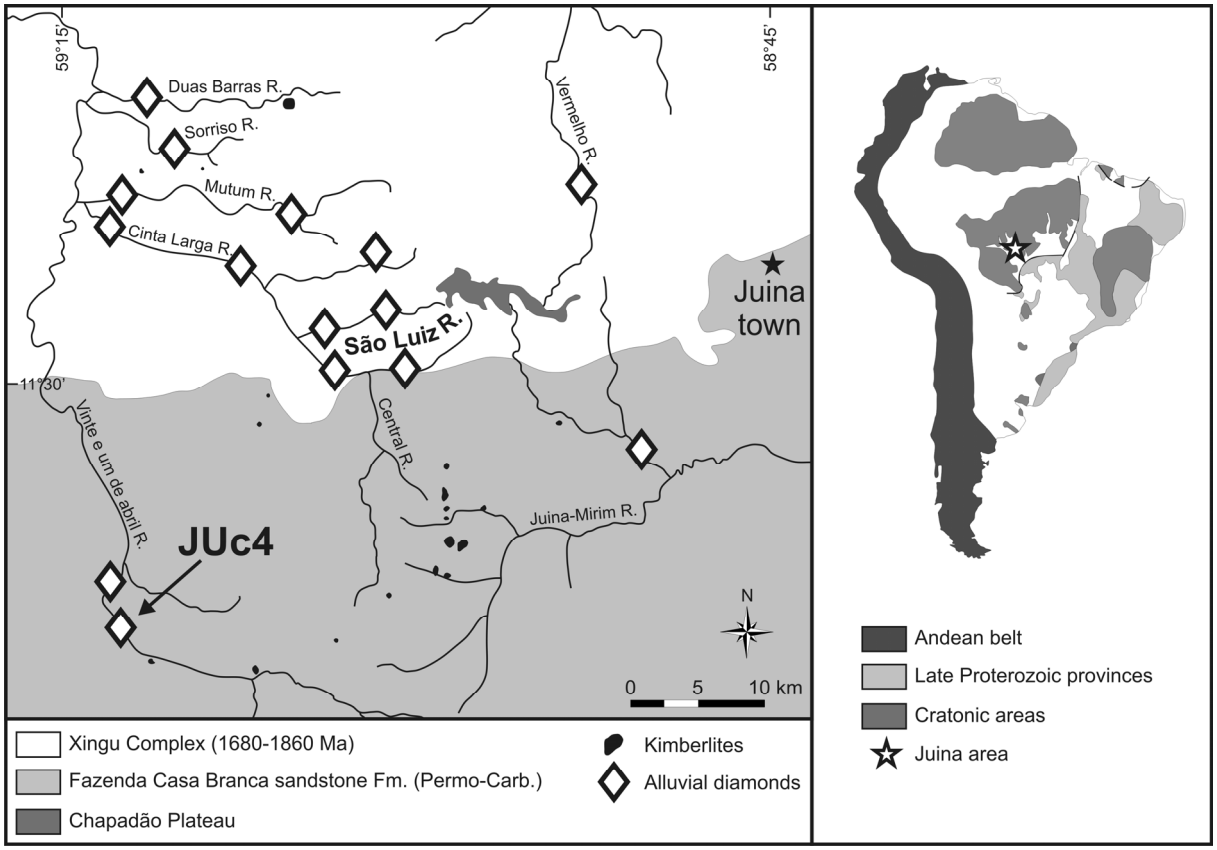

Fig. DR1. Location of sample JUc4 and of kimberlites and alluvial diamond deposits of the Juina area (modified after Bulanova et al., 2010, and Araujo et al., 2013).

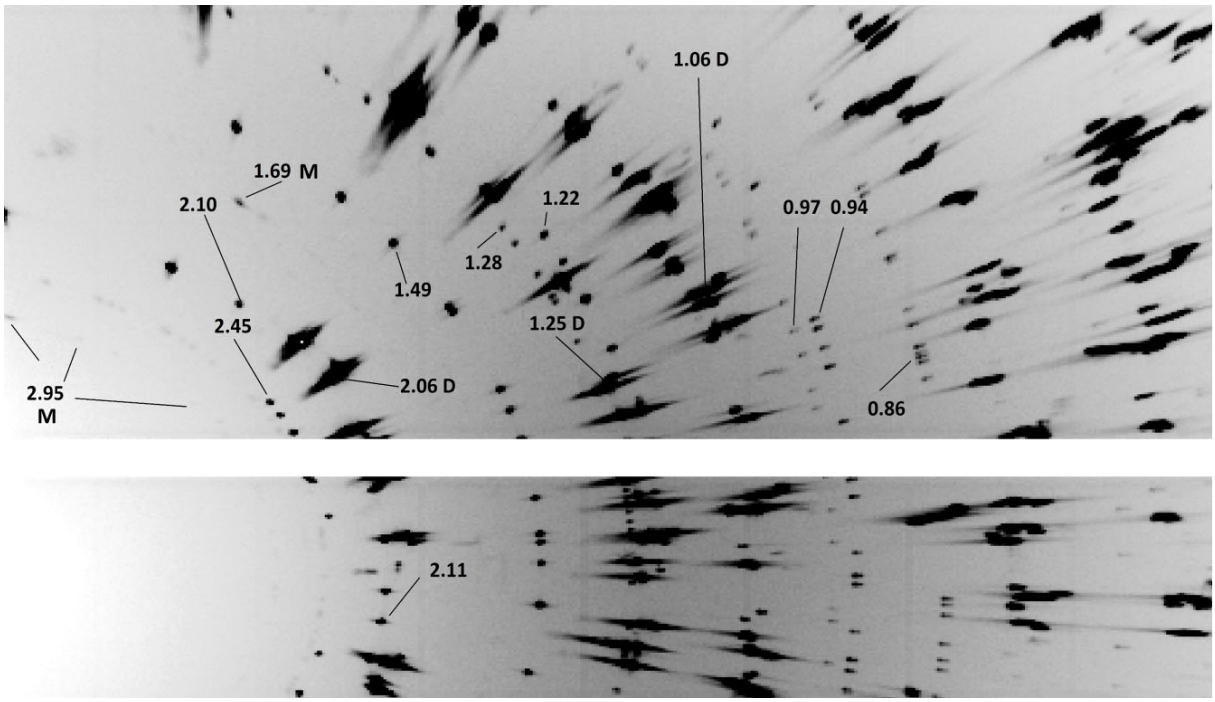

Fig. DR2. Representative diffraction image of an FM inclusion in diamond BZ270. ‘D’ indicates diffraction peaks related to diamond. ‘M’ indicates diffraction peaks consistent with the presence of minor magnesioferrite or magnetite. Other peaks are related to FM. Note that the two main peaks of magnesioferrite/magnetite (113 and 440) overlap peaks 111 (at 2.4-2.5 Å) and 220 (at 1.4-1.5 Å) of FM. Therefore, the identification of magnesioferrite/magnetite is based on the two peaks at 2.95 and 1.69 Å, which do not overlap with any of the FM and diamond peaks.

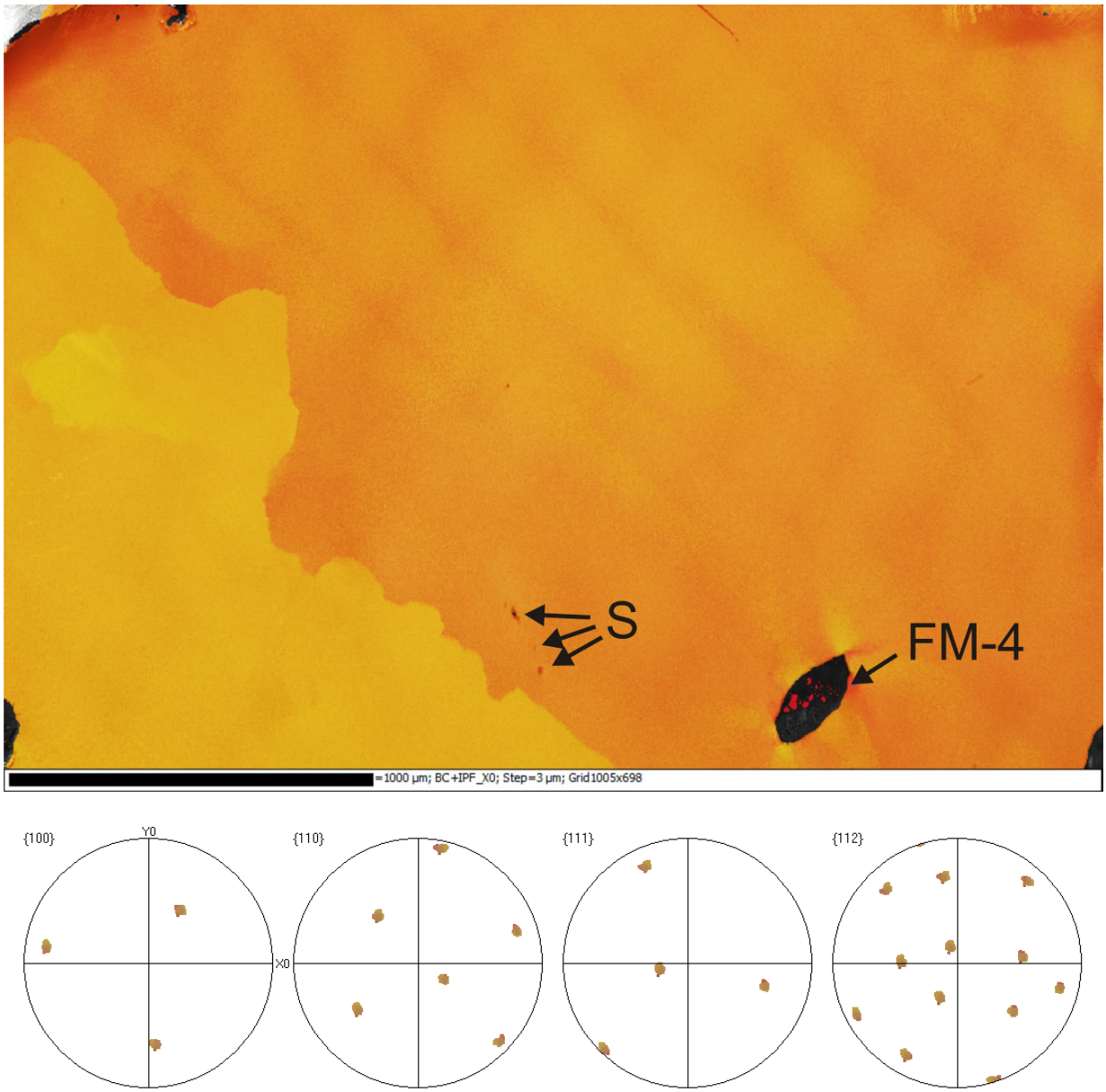

Fig. DR3. EBSD map and pole figure data for diamond BZ270, showing two main subgrains and deformation bands related to plastic deformation. The NW-SE running deformation bands on the right side of the diamond are orthogonal to a {111} pole located along the primitive circle of the pole figure. This suggests that the bands are parallel to a {111} plane, consistent with the activation of {111}<011> slip systems. Misorientation profiles show a crystallographic mismatch along the subgrain boundary visible on the left side of the diamond single crystal of up to 3.5°. Exposed inclusions of FM (n. 4) and Fe-monosulfide (S) are indicated by arrows.

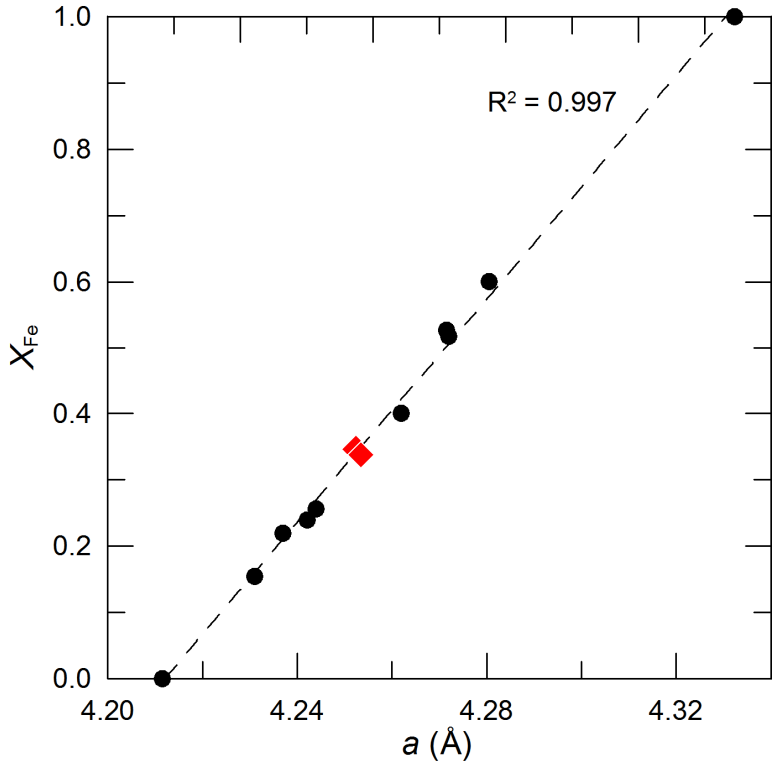

Fig. DR4. Relationship between unit-cell *a* edge and composition in nearly stoichiometric FM from the literature (black dots) and in FM inclusions n. 4 and 5 in diamond BZ270 (red diamonds). Regression line was calculated using the literature data only. Source of data: Hentschel (1970), Rosenhauer et al. (1976), Jackson et al. (1978), Richet et al. (1989), Reeber et al. (1995), Jacobsen et al. (2002).

Microcomputed X-ray tomography of diamond BZ270

2019006 Video DR1.avi

ADDITIONAL REFERENCES CITED

Araujo, D.P., Gaspar, J.C., Bulanova, G.P., Smith, C.B., Kohn, S.C., Walter, M.J., Hauri, E.H. (2013) Juina diamonds from kimberlites and alluvials: a comparison of morphology, spectral characteristics and carbon isotope composition, *in* Pearson, D.G., Grütter, H.S., Harris, J.W., et al., eds., Proceedings of 10th International Kimberlite Conference. Springer, New Delhi Heidelberg New York Dordrecht London, p. 255–269.

Angel, R.J., Finger, L.W., 2011, SINGLE: a program to control single-crystal diffractometers: Journal of Applied Crystallography, v. 44, p. 247–251, doi: 10.1107/S0021889810042305.

Bulanova, G.P., Walter, M.J., Smith, C.B., Kohn, S.C., Armstrong, L.S., Blundy, J., and Gobbo, L., 2010, Mineral inclusions in sublithospheric diamonds from Collier 4 kimberlite pipe, Juina, Brazil: subducted protoliths, carbonated melts and primary kimberlite magmatism: Contributions to Mineralogy and Petrology, v. 160, p. 489–510, doi:10.1007/s00410-010-0490-6.

Cnudde, V., and Boone, M.N., 2013, High-resolution X-ray computed tomography in geosciences: A review of the current technology and applications: Earth-Science Reviews, v. 123, p. 1–17, doi: 10.1016/j.earscirev.2013.04.003.

Hentschel, B., 1970, Stoichiometric FeO as metastable intermediate of the decomposition of wüstite at 225°C: Zeitschrift für Naturforschung A, v. 25, p. 1996–1997.

Jackson, I., Liebermann, R.C., and Ringwood, A.E., 1978, The elastic properties of $(Mg_xFe_{1-x})O$ solid solutions: Physics and Chemistry of Minerals, v. 3, p. 11–31.

Jacobsen, S.D., Reichmann, H.-J., Spetzler, H.A., Mackwell, S.J., Smyth, J.R., Angel, R.J., and McCammon, C.A., 2002, Structure and elasticity of single-crystal (Mg,Fe)O and a new method of generating shear waves for gigahertz ultrasonic interferometry: Journal of Geophysical Research, v. 107, 2037, doi: 10.1029/2001JB000490

Nestola, F., Nimis, P., Ziberna, L., Longo, M., Marzoli, A., Harris, J.W., Manghnani, M.H., and Fedortchouk, Y., 2011, First crystal-structure determination of olivine in diamond: Composition and implications for provenance in the Earth's mantle: Earth and Planetary Science Letters, v. 305, p. 249–255, doi: 10.1016/j.epsl.2011.03.007.

Prawer, S., Nemanich, R.J., 2004, Raman spectroscopy of diamond and doped diamond. Philosophical Transactions: Mathematical, Physical and Engineering Sciences, v. 362, p. 2537–2565, doi: 10.1098/rsta.2004.1451.

Reeber, R.R., Goessel, K., and Wang, K., 1995, Thermal expansion and molar volume of MgO, periclase, from 5 to 2900 K: European Journal of Mineralogy, v. 7, p. 1039–1047.

Richet, P., Mao, H.-K., and Bell, P.M., 1989, Bulk moduli of magnesiowüstites from static compression experiments: Journal of Geophysical Research, v. 94, p. 3037–3045.

Rosenhauer, M., Mao, H.K., and Woermann, E., 1976, Compressibility of magnesiowüstite ($Fe_{0.4}Mg_{0.6}O$) to 264 kbar: Carnegie Institution Washington Year Book, v. 75, p. 513–515.

Sheldrick, G.M., 2008, A short history of SHELX: Acta Crystallographica A, v. 64, p. 112–122, doi: 10.1107/S0108767307043930.